# Cast Component Development for High Cycle Fatigue in the Precision Sand Casting Process (PSCP)

Robert Mackay & Glenn Byczynski
Nemak North America, Southfield, Michigan, USA



## ABSTRACT

The Precision Sand Casting Process (PSCP) is used to manufacture components that typically have complex architectures but also must sustain high cyclical compression and tensile loads in service conditions. Literature generally argues the key to improved tensile and fatigue performance in PSCP is to keep porosity as low as possible. This manuscript outlines the key elements in the current PSCP evolution which have addressed improved high cycle fatigue performance and identifies the areas of research needed in the future to further push secondary aluminum in fatigue performance.

**Keywords**: precision sand casting process, PSCP, high cycle fatigue, cast component development

## INTRODUCTION

Failure due to either tensile or fatigue fracture in service conditions can result in significant warranty costs (engine warranty replacement costs range from 8 to 15K USD). Therefore, a significant portion of the literature about the Precision Sand Casting Process (PSCP) has focused on porosity development and the impact porosity has on tensile and fatigue characteristics.[1-8] Aluminum has demonstrated to be a light weighting option to cast iron and steel, a characteristic which is becoming more important in terms of reaching CAFE (Corporate Average Fuel Economy) for vehicles with Internal Combustion Engines (ICE), Hybrid Electric Vehicles (HEV) and Plug-in Hybrid Electric Vehicles (PHEV) and addressing range anxiety with Battery Electric Vehicles (BEV).

The worldwide automotive landscape is expected to grow from 64M (mainly ICE with limited PHEV and HEV) in 2019, to 86M (ICE, BEV, PHEV and HEV) by 2030. Thus, it is expected that the use of secondary aluminum in PSCP will steadily grow to match future automotive volume projections.

Fatigue fracture failure in components made using the PSCP will most likely result either from a pore exposed on a machining surface, or from a sharp design edge on the casting surface, both of which during loading will produce an elevated stress concentration effect enhancing fatigue fracture probabilities. During component validation, sharp design edge effects may be identified and re-designed/modified in subsequent qualification testing. Thus, final component testing incorporates the necessary design changes eliminating its possible contribution to fatigue failure in service. It is more common that exposed porosity on a machined casting surface will contribute to fracture failure in service conditions. An example of this can be shown in Figure 1a where a fatigue crack has propagated from the trough region of the cut bolt hole thread profile. This is further illustrated in Figure 1b where the schematic illustrates pores being distributed around a tapped and cut bolt hole and one of those pores happens to be at a trough portion of the thread profile. Roll forming, exemplified in Figure 1c, acts to physically compress any possible pores that would be exposed in the thread cut option, removing its potentially elevated stress concentration effect. While high yield stress (YS) is needed for the component design parameter aspects, high plastic elongation (e.g., > 1%) is needed to allow the roll forming process to occur without resulting in fractures.

Roll-forming is implemented in most PSCP applications today (and most engine blocks used in the manuscript) which enhances component durability. However, the fatigue testing outlined in this manuscript still must be conducted as an elevated porosity event in production can impact the barrier to fatigue nucleation that roll-forming offers.

Finally, there needs to be a comment on the casting process used to make automotive components in general. High Pressure Die Casting (HPDC) accounts for nearly 80% of global production of aluminum castings with most of that balance being made using the Gravity Semi-permanent Mold Process (GSPM) and the Precision Sand Casting Process (PSCP). The authors have published previously the difference in the PSCP and HPDC in terms of casting yield, alloys used and expected mechanical performance.[9,10] This will not be discussed here other than for the higher performance applications the PSCP tends to be the process used where mechanical properties are the highest (e.g., UTS > 200 MPa and plastic elongation > 1%).[11]

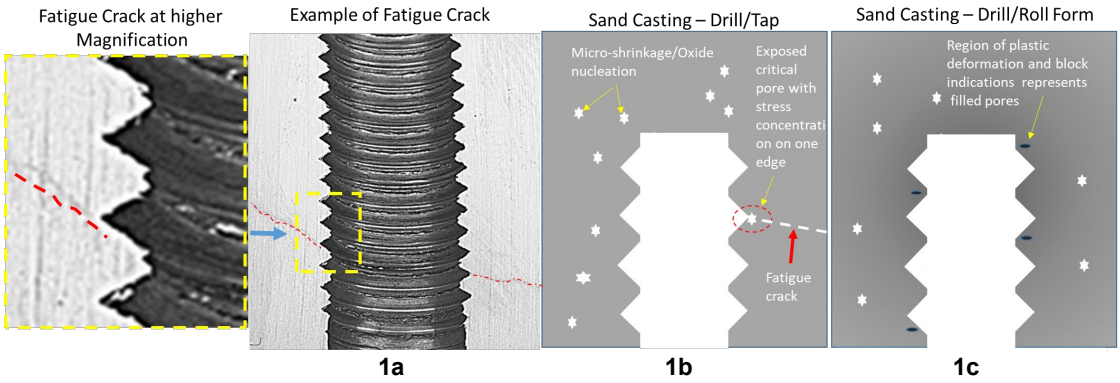


***Figure 1a. Image of a tapped and cut bolt hole which illustrates a fatigue crack which has nucleated from the trough portion of the thread profile. 1b) a schematic thread profile where a pore located at the thread trough, 1c) with roll-forming illustrating how pores opened by the initial hole cut are plastically deformed and closed.[1]***

## CASTING CONDITIONS INVESTIGATED

The castings chronicled for this manuscript were engine blocks made using the Nemak-Cosworth™ process.[9,10] As will be mentioned in the Experimental Methodology section, a template is used to consistently delineate the fatigue and tensile test blank location from the casting bulkhead region. The different conditions in terms of sand type used, casting, alloy, use of a cast iron chill and raw casting weights are shown in Table 1.

The sand type used is either zircon or silica. The historical selection of sand was related to several factors, including density, reclaimability, surface quality and heat extraction capacities. PSCP using zircon can result in a Secondary Dendrite Arm Spacing ($\lambda_2$) reduction of 10 $\mu$m in casting coarseness in non-chilled regions.

The first five casting conditions do not use the chill to refine the microstructure but instead the bulkhead regions are risered which gives rise to the coarse microstructures compared to chilled bulkheads as shown in Figure 2.

For the non-chilled conditions Sr is only added in the W319-V8 + Sr castings (~ 60 ppm, Table 1) and has been shown in previous publications that Sr promotes a larger amount of dispersed microshrinkage indications which impair fatigue and tensile properties.[1,9,12] In chilled applications Sr was re-introduced not only with the aim of refining Si morphology (improved machinability) but to reduce the severity of gross shrinkage indications as measured using the ASTM E155 radiographic standard.

In addition, the dispersed microshrinkage that forms due to the Sr concentrations is minimized by the heat extraction of the chill.

The casting yield is higher without a chill than for these castings which are chilled. The reason for this has to do with the fact that the risers in chilled condition must be attached to the head deck instead of the bulkhead (Figure 2). Head deck connected risers tend to have small ingates requiring the risers to be larger, and they promote the directional solidification the chilled process requires.[1,9,10]

Table 2 outlines the Thermal Sand Removal (TSR), conditions, quench rates, solution conditions and the following age conditions used. Heat treatment conditions tend to not impact fatigue results in the way critical flaws do.[6-8] However, heat treatment does impact tensile properties as they are controlled by $\alpha$-Al matrix hardness, in addition to the effects of both the secondary phase constituent size and the magnitude of over-all porosity.

Removal of the solution stage in two of the casting conditions was covered in previous publications, where the age temperature adjustment can be made to achieve the same tensile mechanical result with the solution stage.[11,14] Quenching after solution was by forced air unless the blocks had pressed in liners (e.g., W319-V8 and U328-V8 engine blocks) then water mist quenching was used.

***Table 1. Summary of Casting Weights, Yield, Sand Type, Chill Condition and Melt Quality***

| Non-chilled, Bulkhead Risered | | | | | | Chilled Bulkhead | | |
|---|---|---|---|---|---|---|---|---|
| Metric | W319-V8 + Sr | W319-V8 | W319-V6 | V354-V6 | U328-V8 | V354-V6+Chill1+Sr | V354-I4+Chill2+Sr | V354-V6+Chill2+Sr |
| Engine Block + Risers Weight (Kgs) | 63.5 | 63.5 | 45.8 | 45.8 | 63.5 | 54.8 | 36.5 | 54.4 |
| Casting Yield | 70% | 70% | 70% | 70% | 70% | 55% | 55% | 55% |
| Sand - Mold | Zircon | Zircon | Zircon | Zircon | Zircon | Silica | Silica | Silica |
| Bulkhead Contact | Zircon | Zircon | Zircon | Zircon | Zircon | Breadloaf - Cast iron | Wrapped-Cast Iron | Wrapped-Cast Iron |
| Rigging (ingate and risers) | Bulkhead Risered | Bulkhead Risered | Bulkhead Risered | Bulkhead Risered | Bulkhead Risered | Head Deck Risered | Head Deck Risered | Head Deck Risered |
| Casting Temp. | 760°C | 760°C | 740°C | 740°C | 760°C | 725°C | 725°C | 725°C |
| Sr Concentration | 60 ppm | > 20 ppm | > 20 ppm | > 20 ppm | > 20 ppm | 60 ppm | 150 ppm | 125 ppm |

***Table 2. Thermal Sand Removal and Thermal Processing***

| Non-chilled, bulkhead Risered | | | | | | Chilled Bulkhead | | |
|---|---|---|---|---|---|---|---|---|
| Metric | W319-V8 + Sr | W319-V8 | W319-V6 | V354-V6 | U328-V8 | V354-V6+Chill1+Sr | V354-I4+Chill2+Sr | V354-V6+Chill2+Sr |
| Liner Condition | Pressed In | Pressed In | Cast In | Cast In | Pressed In | Cast In | Cast In | Cast In |
| TSR | 499°C @ 4.5 hours | 499°C @ 4.5 hours | 499°C @ 4.5 hours | 499°C @ 4.5 hours | 499°C @ 4.5 hours | 485°C @ 4.5 hours | 485°C @ 4.5 hours | 485°C @ 4.5 hours |
| TSR Quench | froced air | froced air | froced air | froced air | froced air | froced air | froced air | froced air |
| Sol | 495°C @ 7.0 hours | 495°C @ 7.0 hours | NA | NA | 505°C @ 5 hours | 485°C @ 7.0 hours | 485°C @ 7.0 hours | 485°C @ 7.0 hours |
| Sol Quench | 90°C water | 90°C water | NA | NA | 90°C water | forced air | forced air | forced air |
| Age | 270°C | 270°C | 265°C | 250°C | 230°C | 240°C | 240°C | 240°C |

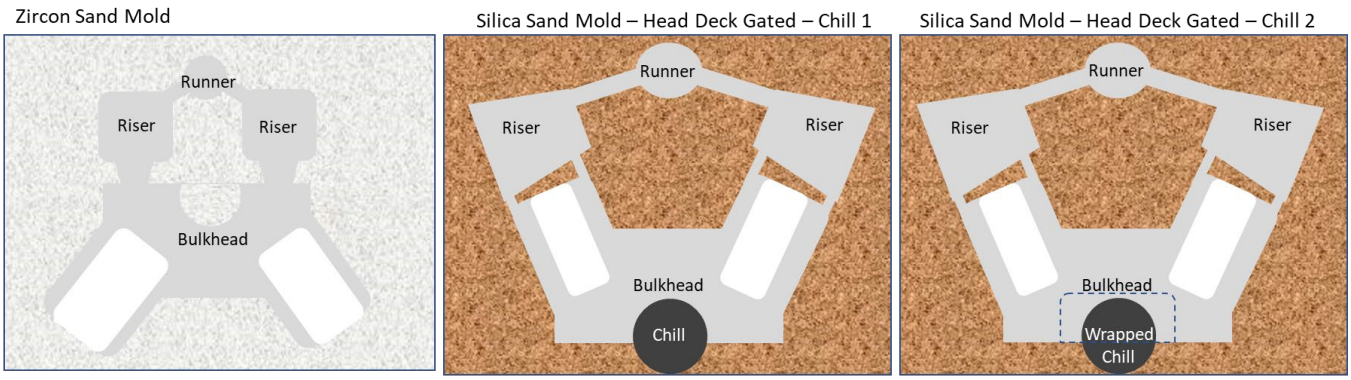


***Figure 2. The three configurations for casting engine blocks used in the current study. Chill1 has approximately half of the contact area with the bulkhead Chill2. Zircon mold configurations have a riser adjacent to the bulkhead. Note the tensile/fatigue test bar is extracted from the bulkhead. Grain refining is conducted by the addition of Tibor in the runner.***

## EXPERIMENTAL METHODOLOGY

Liquid metal treatment for the Nemak-Cosworth™ process has been described in more detail elsewhere[9] however the key points are that the aluminum alloy after breakdown undergoes rotary degassing and filtration before the casting station.

The target dissolved level of hydrogen must be below 0.10 $H_2$ $cm^3/100$ g Al (RPT ≥ 2.70 grams/$cm^3$) and chemistry verified on a calibrated Optical Emission Spectroscopy (OES). The chemistry limits of the alloys used to make the engine blocks are shown in Table 1.

Trace elements are also kept within limits as prescribed under purchase specification standards. Not listed in Table 1 for brevity, the max limits for trace elements are: Pb is ≤ 50 ppm, Sn ≤ 40 ppm, Ca, Na, P are kept ≤ 20 ppm and finally B and Sb are kept ≤ 10 ppm. Sr concentrations are made by addition to the casting station melt bath (to minimize fading) and target levels for each casting condition are outlined in Table 1.

In terms of grain refiner additions, a Tibor rod (Al-5Ti-1B) is added in-mold via the runner system. As liquid metal begins to fill the mold package the Tibor gradually dissolves into the mold itself. The principal purpose for using Tibor is to reduce the size of the columnar grains which form particularly from the chilled conditions.

## MECHANICAL TESTING PROTOCOLS

All fatigue and tensile test bars are extracted from the production castings made and outlined in this manuscript. To minimize any scatter in testing results a plastic template is designed and is used to draw the blank outline first, then sectioned on a band saw so that final mechanical test bar fabricated on a machining lathe can occur. Figure 3a shows an image of a casting section with the plastic template on top. The importance of the template is illustrated by the $l_2$ array indicated in Figure 3b.

***Figure 3a. Example of the template used to ensure the exact placement of tensile and fatigue test blanks within the bulkhead.***

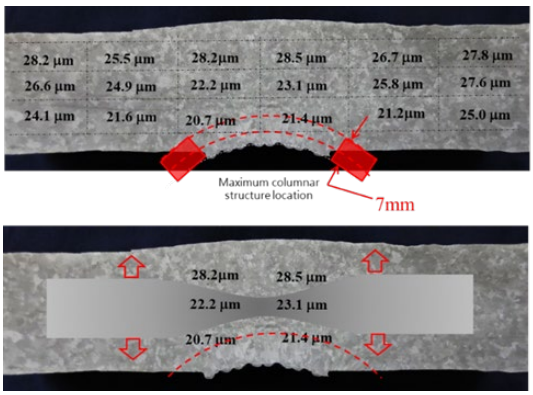


***Figure 3b. Area of extraction of both fatigue and tensile test bar blanks. The values listed in the array reflect the $\lambda_2$ measured.***

***Table 3. List of Alloy Compositions (wt.%)***

| Alloy | | Si | Fe | Cu | Mn | Mg | Ni | Zn | Ti |
|---|---|---|---|---|---|---|---|---|---|
| W319 | Max | 8.00 | 0.40 | 3.80 | 0.30 | 0.50 | 0.30 | 1.00 | 0.25 |
| | Min | 6.50 | | 2.20 | 0.20 | 0.05 | | | |
| U328 | Max | 9.50 | 0.40 | 1.50 | 0.30 | 0.50 | 0.30 | 1.00 | 0.25 |
| | Min | 8.50 | | 0.50 | 0.20 | 0.05 | | | |
| V354 | Max | 8.75 | 0.59 | 2.60 | 0.40 | 0.40 | | 0.80 | 0.18 |
| | Min | 8.10 | | 2.00 | | 0.30 | | 0.40 | |

## TENSILE TESTING

The tensile test bars were fabricated and tested as per the ASTM B557 protocol. The Nemak Engineering Centre's Metallurgical Lab was used to conduct all tensile testing on a United Test Systems (SFM–60) mechanical workstation. A completed test (at the point of fracture) took approximately 5 minutes. A strain gauge extensometer was attached to the tensile test samples for the measurement of elongation. After the test was conducted the 0.2% offset Yield Stress (YS), Ultimate Tensile Stress (UTS), and Plastic Elongation (PE) were measured as defined in the ASTM B557 specification. Tensile testing at the Nemak Engineering Center was accredited to ISO/IEC 17025 by A2LA (certificate: 2478.01).

## FATIGUE TESTING PROTOCOLS

Fatigue test sample testing was carried out as per the ASTM E466-96 protocol. TestStar™ IIs fatigue software by MTS was used to monitor the sinusoidal axial fatigue at a frequency of 98Hz. The stress ratio was R = -1, (R is defined as $\square_{min}/\square_{max}$). Maintaining a test temperature of 150C (302F) was done using a resistance heater tape material (Omega) which is in direct contact with the test specimen. Temperature is monitored by a K-type thermocouple that is held in place on the reduced gauge section using 3M glass fiber electrical tape. It typically takes 3 to 5 minutes for the reduced gauge section to reach the target temperature.

The alignment process of the fatigue test frame performed is meant to address two types of possible misalignment possibilities: concentric and angular. The fatigue test frames are equipped with an alignment collar (MTS Model 609) that allows alignment in conjunction with a specimen fitted with 12 strain gauges that relates to a computerized alignment data acquisition and analysis system (MTS 709). This is the system that is used to align the fatigue frames in accordance with ASTM E1012-05. Fatigue testing was carried out under contract at the Element Wixom facility and is accredited to ISO/IEC 17025 by A2LA (certificate: 0098.07).

The type of fatigue protocol used was the staircase method. The staircase method can be described as follows: If a life goal of $10^7$ cycles without a failure occurred then it is considered a run-out for a given targeted alternating stress. A subsequent test would be conducted on a fresh fatigue test sample at an

incrementally higher alternating stress. A sample not achieving the $10^7$-cycle life goal is considered a failed test, and results in the very next sample being tested at an incrementally lower alternating stress. The total fatigue samples cycled for this manuscript is thirty (30) or thirty-six (36) depending on the number of castings made for product development. Customer requirements for mean staircase fatigue testing are 30 as a minimum for statistical reasons (e.g., -3□ determination).

The mean stress of the staircase study would be determined by taking the average stress of all the fatigue test samples which failed (higher value of stress) or all the fatigue test samples which passed (lower value of stress), whichever is lower in number. The logic of using the lower number of sample test results is to negate the effect of a poor estimate of the starting stress.

Figure 4 shows the example of the staircase plot for a W319 alloy where 15 samples were failures and 21 were run-outs. Thus, the failures in Figure 4 were used to produce a mean alternating fatigue result of 52.4 ± 3.0 MPa (-3s = 43 MPa). Figure 4 also shows the more succinct bar graph method which is used to represent the fatigue staircase data in the manuscript.

## METALLOGRAPHY

Metallography was done in the reduced gauge section of the completed fatigue test sample (Figure 5). Since both tensile and fatigue reduced gauge sections are from the same region of the bulkhead due to the template outlined in Figure 3a, the same metallography was not repeated on tensile test samples.

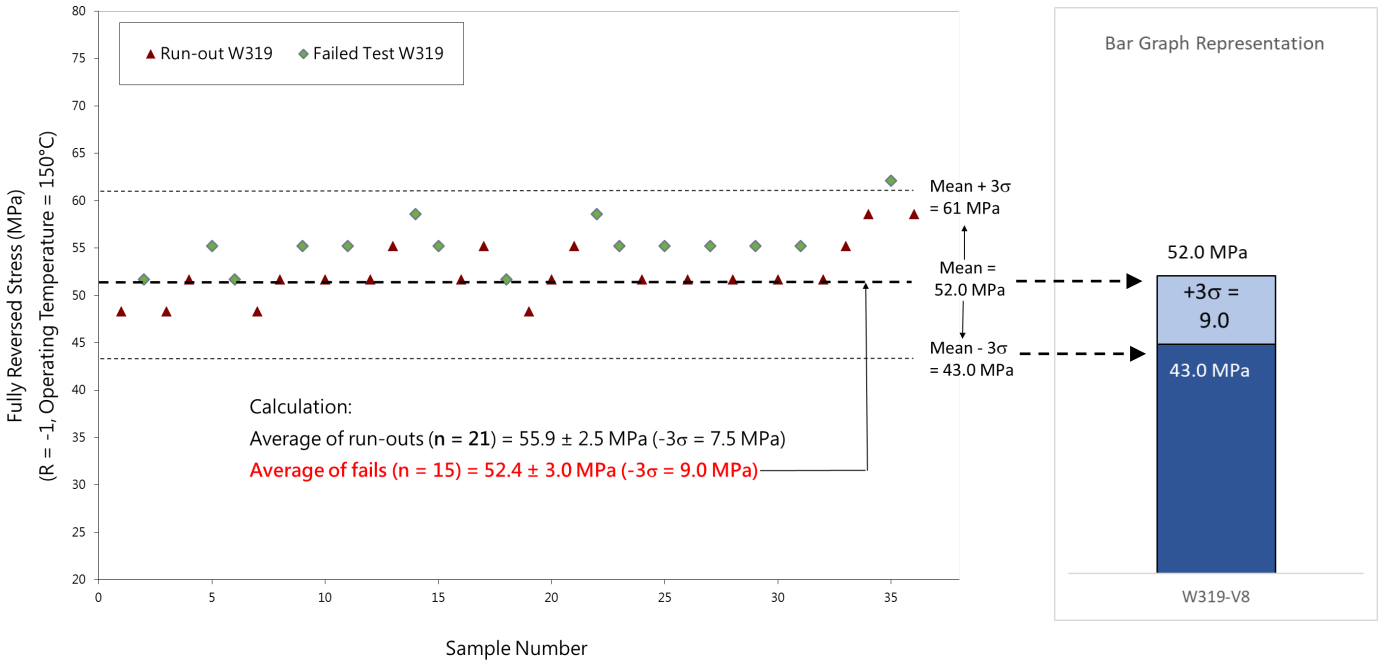


***Figure 4. The method for determination of mean alternating stress from a staircase plot and the -3σ calculation. In the above example the W319 alloy achieved a mean alternating stress value of 52.0 MPa (calculated from 15 samples which were fails) along with their +3σ and -3σ values. The -3σ value is most often cited as it is related to the lowest probable value of alternating stress, which fatigue failure is considered not statistically possible within 99.99%. The bar graph representation is included on the right in the above figure.***

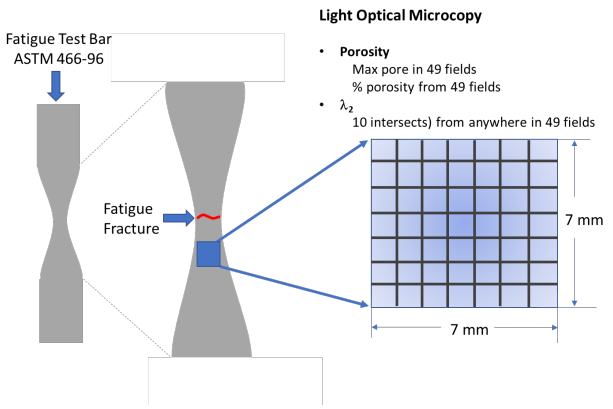


***Figure 5. Metallographic examination was done in the area just below the fatigue fracture surface.***

Metallography was conducted on an Olympus IX70 Light Optical Microscope system. Porosity and □2 were quantified with the aid of an Image Analysis software by CLEMEX (Version 3.5.020 F). Average max pore size and percent porosity (%) assessment was performed on a 49-field grid array (7mm x 7 mm) at a magnification of 50x.

The length measurement to support □2 determination was checked against a calibration scale (S/N: SM-2-0064, 99.8□m measured against a 100□m scale). At a magnification of 50x several lines are drawn which orthogonally intersect at least five to six secondary dendrites. This was repeated 10 times to determine the average value for $\lambda_2$. This 10-time measurement for $\lambda_2$ was done within the same metallographic grid as for porosity (Figure 5).

## RESULTS

Figure 6 shows the summary of the tensile test results from the bulkhead. Due to the integrated chill conditions Yield Stress (YS), Ultimate Tensile Strength (UTS) and Plastic Elongation (PE) are all much higher than for the non-chilled conditions. This is due to the fact that these tensile tests bars have lower porosity, lower size of secondary phase constituents (e.g., Si platelets of the Al-Si eutectic, and the a-$Al_{15}(Fe,Mn,Cr)_3Si_2$ script phase) and a more plastic and refined α-Al matrix.[1,2-4,14-19] Further to this the α-Al matrix will have more retained solute which will produce a faster age response during heat treatment.[1,11,19] Without an integrated chill in the bulkhead both porosity and secondary phase constituents are larger, and the α-Al matrix is softer due to the lower level of retained solute which results in a slower age response.[1,11,19]

Figure 7 shows the summary of the fatigue staircase performance in the form of a bar plot where the -3s value is integrated for brevity. All non-chill conditions have a mean alternating fatigue stress ranging from 34.5 MPa up to 76.4 MPa while chilled bulkheads result from 58.4 MPa up to 91.8 MPa.

Figure 8 shows the representative microstructures (100X magnification) for all fatigue test bars from all casting conditions investigated. From Figure 8 the coarse structure is shown as reflected by the larger $l_2$ in the non-chilled conditions and only slight Si refinement for the W319-V8 + Sr condition exists (60 ppm). In chilled conditions there is both the refinement in $l_2$ and Si morphology due to the rapid heat extraction and elevated Sr concentrations (60 – 150 ppm).

Figure 9 shows the corresponding average max pore size and percentage porosity, and Figure 10 shows the $l_2$ values, both from the reduced gauge section of fatigue bars.

Figure 9 shows that the porosity values drop from left to right of the non-chilled conditions and this is due to the freezing range effects of alloy chemistry. The non-chilled condition W319-V8 + Sr contains 60 ppm Sr, which is limited to only trace level amounts (≥ 20 ppm) in the rest of the non-chilled conditions. Elevated Sr concentrations are known for increasing not only the number of pores, but making them larger, in addition to the Si platelet change from acicular to fibrous. Strontium does extend the freezing range but also changes the Al-Si nucleation kinetics which promotes more heterogeneous nucleation sites for pores.[12,19-21]

In chilled conditions porosity is lower because of the rapid heat extraction impact of the chill itself. However, in these conditions the Sr concentration was targeted between 60 to 150 ppm. Due to the chill, porosity was similar the Sr-free non-chilled conditions (e.g., compare W319-V6 to V354-V6+Chill1+Sr), but the elevated Sr concentrations allowed the refinement of Si platelets away from the chill which was utilized for improved machining characteristics.

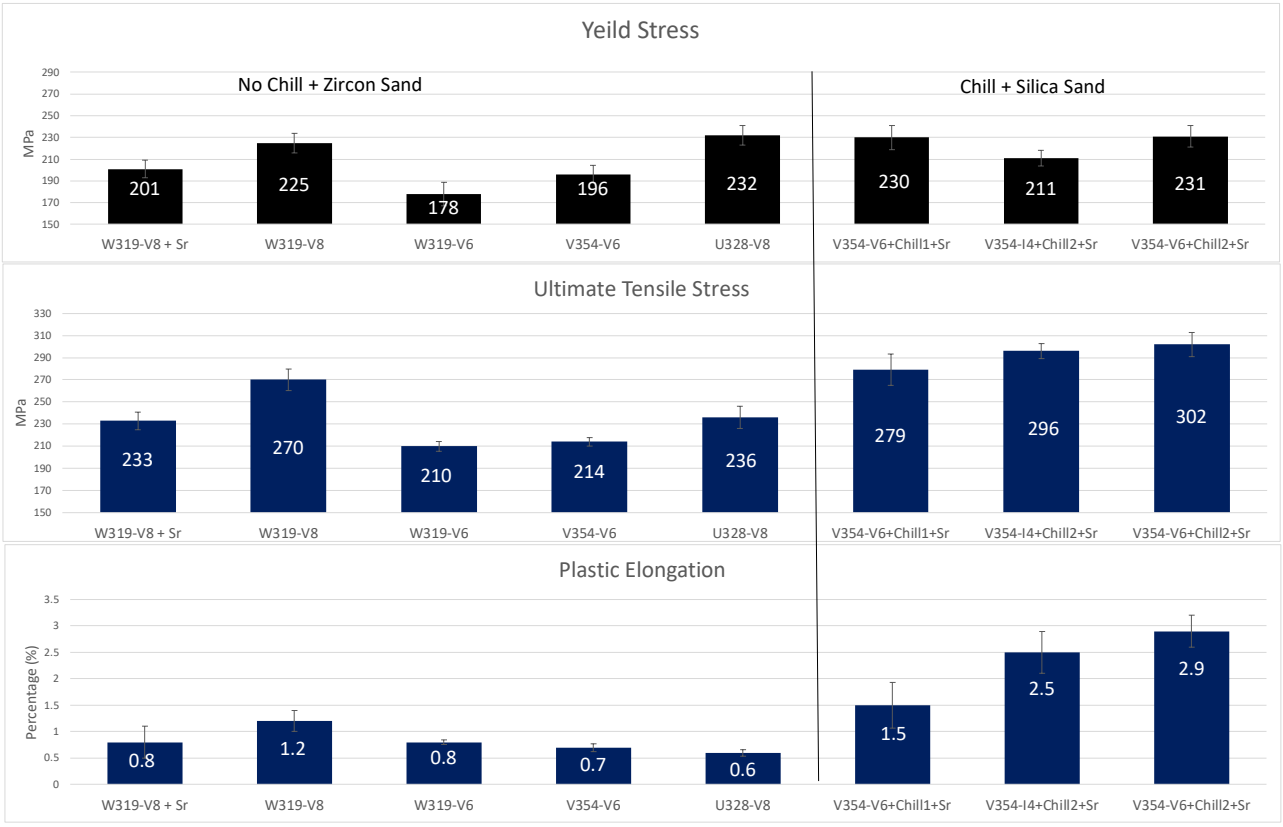


***Figure 6. Summary of tensile results. N = 30 for each condition with individual error bars.***

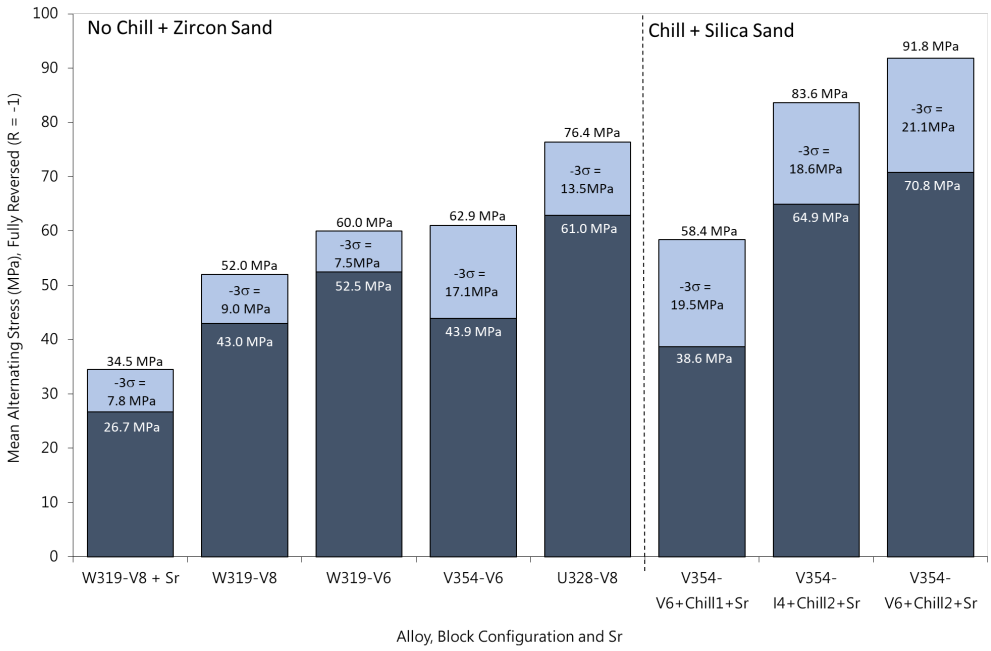


***Figure 7. Summary of the mean fatigue stress along with -3σ calculation as illustrated in Figure 3 (W319 example used, n=36). Bar graph format representation is described in Figure 4.***

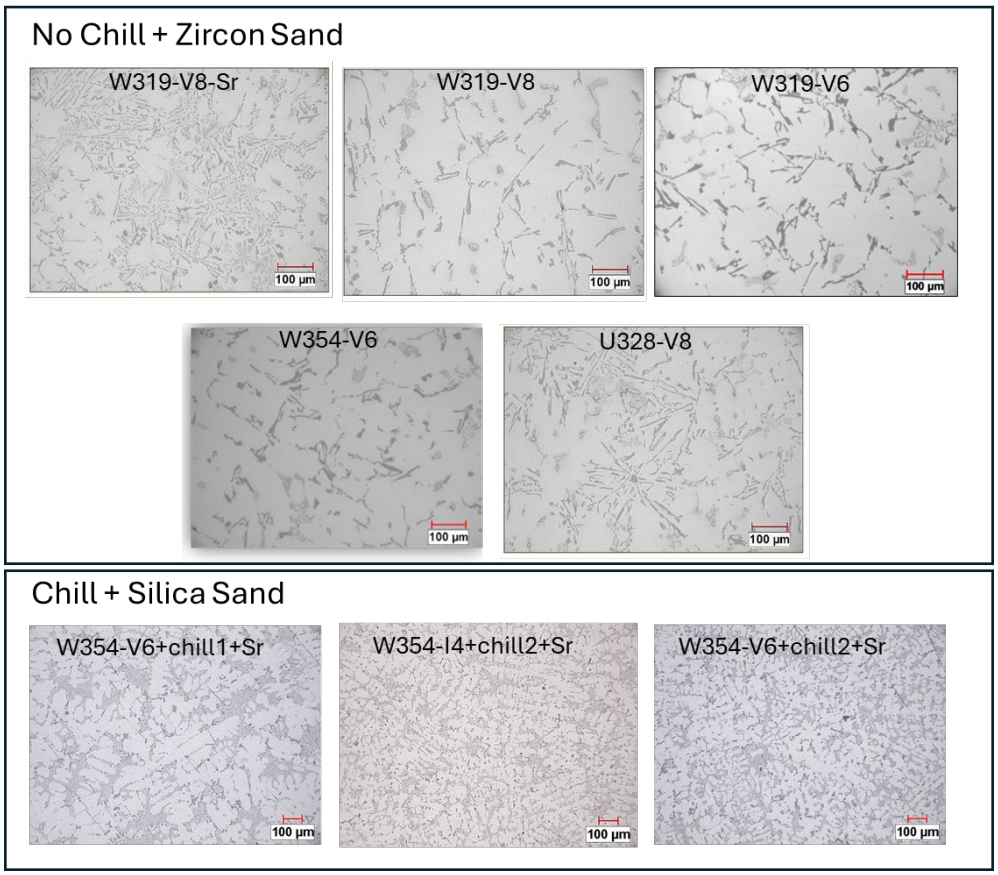


***Figure 8. A representative microstructure of each alloy studied in this manuscript. Non-chilled conditions show the larger $\lambda_2$ values while in chilled conditions we see smaller $\lambda_2$ (Figure 10 for measured $\lambda_2$ values). Secondary phase constituents such $Al_2Cu$, $Mg_2Si$, $\alpha$-$Al_{15}(Fe,Mn,Cr)_3Si_2$, $\alpha$-$Al_8Fe_2Si$ and $\alpha$-$Al_{12}Fe_3Si_2$ were seen in all alloys, however $Al_5FeSi$ platelets are essentially absent due to the Mn concentrations meeting Mn/Fe (≥0.7) thresholds.[15,16,19]***

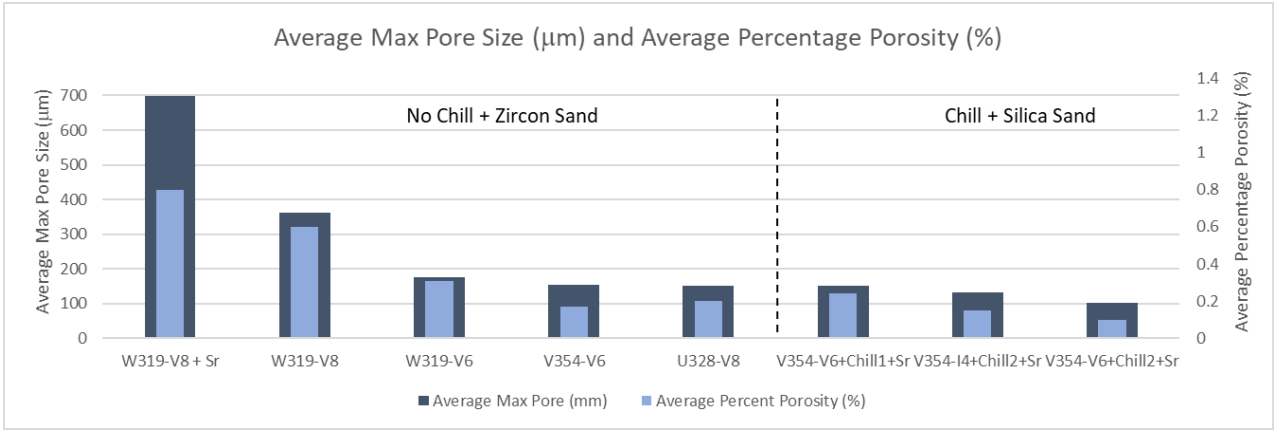


***Figure 9. Summary of casting conditions and resulting bulkhead microstructure (n = 5).***

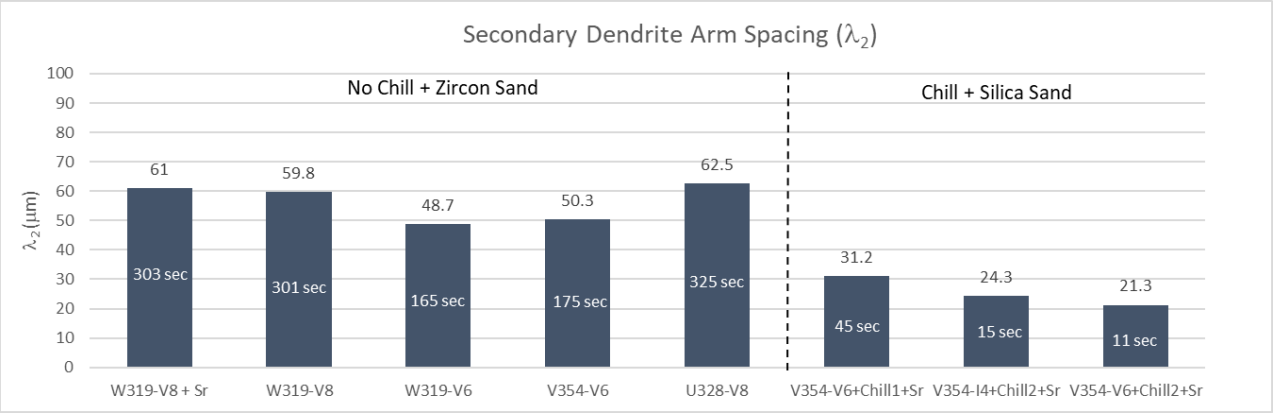


***Figure 10. Summary of the $\lambda_2$ values as measured below the fracture surface of the fatigue test bar (n = 5). Using the previously reported relationship: $\lambda_2 = 10.85t_f^{0.30}$[Ref. 1], where solidification time ($t_f$) can be approximated. Solidification time is indicated by the numerical value in white font in the bar graph.***

Figure 10 shows that in non-chilled conditions the $l_2$ values range from 48 to slightly above 60 mm. Using $\lambda_2 = 10.85t_f^{0.30}$[Ref. 1], where $t_f$ is solidification time, implies that it takes from 165 to 303 seconds to completely freeze in the bulkhead. With chilled conditions $\lambda_2$ drops dramatically to 31 mm for Chill1 condition, or lower with the Chill2 condition at 21 to 24 mm, translating into a calculated solidification times from 45 seconds to 11-15 seconds, respectively.

Referencing the metallographic data from the fatigue test bar in Figures 9 and 10 we can see that in all cases a high $\lambda_2$ value in non-chilled conditions is due to its low solidification rate, but the porosity result found for non-chilled U328-V8 appears to be significantly smaller and closer to the porosity values seen for chilled bulkhead conditions. The reason for this is that the freezing range of the U328-V8 is the shortest of all the alloys investigated by 30°C (54°F).[19] However, due to the coarseness of the microstructure in terms of $\lambda_2$ and secondary phase constituent sizes for the U328-V8 condition the mechanical properties (UTS, YS and PE) are lower and are more in line with the rest of the non-chilled bulkhead testing results. Thus, the lower porosity, due to the shortened freezing range, is the reason why fatigue staircase properties of the U328-V8 condition are more closely matched to chilled conditions, but microstructural coarseness results in tensile properties being more closely match non-chilled conditions.

A final point that must be highlighted: the integrated bulkhead chill is needed to support the lower porosity reduction for improved fatigue requirements, and the above 1% in PE is required for roll-forming threads. For the U328-V8 castings having lower tensile mechanical properties (PE = 0.72 ± 0.2%, Figure 6), risk for small fractures may be encountered when implementing roll-forming.

## IMPACT OF PRINCIPLE ELEMENTS – Si & Cu

The U328-V8 alloy has the highest fatigue performance of the Zircon & non-chilled conditions. The lower porosity results from the fact that the freezing range of the U328 alloy is shortened by 30°C (54°F) due to the combination of higher Si and lower Cu concentrations.[19] The higher Si concentrations work to lower the Liquidus point, and the Cu concentrations elevates the Solidus.[19] The higher Si concentrations also promote the higher volume fraction of the Al-Si eutectic phase which has a lower volumetric contraction during the solidification range which in term reduces the hydrostatic stress build-up imposed by the contracting a-Al dendrite volume fraction.[1,22,23] Conversely, the W319 alloy used in the non-chilled castings have lower Si and higher Cu concentrations which extend the freezing range and has a lower volume fraction of the Al-Si eutectic phase and a higher volume fraction of the a-Al dendrite phase.[1,22,23]

For the chilled conditions only the V354 alloy was used and the main difference between the three variants was either the level of Sr or the thermal mass capacity of the chill. The highest value for the staircase fatigue result was for the V354-V6+Chill2+Sr, which from Figure 10 has the lowest $\lambda_2$, and from Figure 9 has the lowest average max and percentage of porosity. V354 alloy has nearly the same Si concentrations as the U328 alloy, which reduces the amount of primary a-Al dendrite volume fraction and increases the Al-Si eutectic volume fraction, but with the higher Cu concentrations in the V354 alloy, the post eutectic multi-phase nucleation and solidus is extended further to a lower temperature, extending the freezing range.[22,23]

## Sr CONCENTRATIONS & TRACE ELEMENTS

The impact of Sr has been shown to affect fatigue performance when comparing the W319-V8 + Sr (60 ppm Sr) to the W319-V8 conditions (< 20 ppm Sr) in Figure 7. The effect was previously reported,[9,10,12] where larger bulk shrinkage (S rating on the ASTM E155 radiographic

standard) was suppressed with Sr additions but at the expense of increasing dispersed microshrinkage porosity. Eliminating bulk shrinkage is critical as it can contribute to the failure to meet required pressure tightness in quality inspections. However, if Sr is added there is a downside to both tensile and mean alternating fatigue performance. The dispersed microshrinkage defects are usually the very defect which nucleates fatigue cracks and thus can result in failures at lower alternating stresses.[1-3,7,8,13,24] This increase in microporosity on tensile properties is also similarly reflected by comparing the tensile results between the W319-V8 + Sr and W319-V8 casting conditions in Figure 6. Despite the potential beneficial effects of an improved refinement of the Si phase morphology on tensile performance, it was not enough to counter the stress concentration effects of the dispersed microshrinkage.

The impact of Sr can be further illustrated by reviewing the fatigue staircase for V354-V6 (≤ 20 ppm) and the V354-V6+Chill1 + Sr (60 ppm) in Figure 7. Despite having a chill, the elevated Sr concentrations elevate the severity of porosity enough to nullify the chill's impact on fatigue performance, but the elevated Sr will also refine Si morphology away from the chill, improving machining conditions. To improve the fatigue performance, the chill's thermal mass capacity must increase (Chill2 has 50% more contact area than Chill1). Not only does the solidification rate increase (Figure 10) but the Sr target can be adjusted to an even higher level, helping further with Si platelet refinement away from the chill for further improved machining characteristics. However, when comparing the V354-I4+Chill2 +Sr (150 ppm) and V354-V6+Chill2 + Sr (125 ppm) in terms of tensile performance in Figure 6, fatigue performance in Figure 7, and the slightly higher porosity result as shown in Figure 9, we can see the Sr target of 150 ppm was too high. Targeting to 125 ppm Sr provided a better balance between the induced dispersed microshrinkage and the chills power to minimize the dispersed microshrinkage.

While the heat treat regimes used for all of the casting conditions indicate that a Thermal Sand Removal (TSR) followed by a Solution stage, both at either 499C (930F) or at 485C (905F) (Table 2) is not enough in high Sr conditions to promote Si spheroidization. Silica spheroidization will typically be seen in 356/357 alloys as they undergo TSR/Solution temperatures in the range of 515-530C (959-986F) where the kinetics for spheroidization are more advantageous. The alloys studied in this manuscript have solidus temperatures much lower. The V354 alloy for example has a solidus at 507C (945F),[25] which is the reason why the TSR and Solution temperatures as shown in table 2 are much lower than for the 356/357 alloys. Thus, to promote any type of Si spheroidization in the alloys discussed in this manuscript the deleterious impact of incipient melting would occur compromising tensile properties.[16]

The trace elements specified in the Experimental Methodology section were kept within the same level for all the alloys studied in this work. The limits specified for these trace elements are set at low levels so that their impact (e.g., Si platelet morphology changes with elevated Na and Ca concentrations above 20 ppm) does not erroneously skew results.

## Fe CONCENTRATIONS

Fe concentration will be delt with separately as it is one of the most critical elements to limit during manufacturing of secondary alloys. In PSCP applications the Mn concentrations are targeted so that the ratio with the Fe concentrations is between 0.5 and 0.7. This ensures that the formation of $\alpha$-$Al_{15}(Fe,Mn,Cr)_3Si_2$ script phase is promoted over the $\beta$-$Al_5FeSi$ platelet phase.[15,16,19] From Table 1 the maximum Fe concentration permitted is 0.40wt% for non-chilled conditions and extends higher to 0.60wt.% in chilled conditions.

While the maximum Fe concentrations in themselves have not been linked to fatigue performance issues, but more for tensile performance, it is worth pointing out that the Fe differences usually can significantly impact alloy costs. The elevated Fe concentrations allowed for chilled applications resulted in an approximately 0.10 US/lbs. cost reduction for the alloy which can offset somewhat the cost of the chill system required for the chilled process. The cost benefit due to higher Fe concentrations could not be applied to non-chilled conditions because the larger sizes of the $\alpha$-$Al_{15}(Fe,Mn,Cr)_3Si_2$ script could provide greater inter-dendritic feeding issues, elevating porosity, which could have an impact on both tensile and fatigue performance,[1,16] and finally machining characteristics.

## SAND TYPE

As indicated in the Experimental Methodology section there can be a drop of approximately 10 μm in terms of $\lambda_2$ if zircon is used compared to silica in coarse sections of the casting such as the head deck and head bolts.

The casting conditions which used zircon also did not have a chill. The implementation of silica sand was meant to address the dwindling supplies of zircon, and the chill was incorporated as a compensating factor. However, as mentioned the true impact of zircon over silica sand is in non-chill coarse microstructure regions. This impact may have only been seen if the manuscript had a non-chilled silica molded casting version cast where the bulkhead region would potentially see an increase of $\lambda_2$ from 48-60 mm to 58-70 mm (using Figure 10 as a reference). Thus, for these same non-chilled silica molded castings would

also have higher porosity, and consequently even lower mean alternating fatigue strength.

The authors at the end of the manuscript will highlight all the factors needed to drive down porosity but the sand type used may only be academic unless a new type of sand with high heat extraction and low surface roughness could be cost effectively implemented.

### CHILL SIZE

The larger the thermal mass of the chill, the larger the amount of heat can be extracted from the bulkhead inevitably drives down both porosity and $\lambda_2$. This has been reflected when viewing the difference between V354-V6-Chill1 + Sr and V354-V6-Chill2 + Sr conditions which are the same V6 casting, but Chill2 has 50% more contact area. This results in a slight drop in porosity in Figure 9 and a 10 mm drop in $\lambda_2$ as shown in Figure 10.

### BLOCK SIZE/WEIGHT

The impact of the casting size (engine block + rigging) can have an impact on the over-all solidification rate on the bulkhead if a chill is not used. The W319-V8+Sr, W319-V8 and U328-V8 castings have a mass of 63.5 Kgs, while the W319-V6 and V354-V6 have a mass of 43.8 kgs. The nearly 20 kgs difference in mass results in a nearly 10 μm increase in $\lambda_2$ values for the bulkhead. Using the $\lambda_2$ values we can also calculate the solidification time which reveals that the nearly 30% more massive casting takes nearly an additional 140 seconds to completely solidify in the bulkhead.

In chilled conditions the impact of casting weight appears to have limited effect on both porosity and $\lambda_2$ which in turn had a limited impact on fatigue performance. The chill is initially at or near room temperature during casting, resulting in a significant heat extraction which locks in the bulkhead microstructure quickly (within 45 seconds or less). Comparison of the V354-I4 Chill2 + Sr (36.5 kgs.) and V354-V6 + Sr Chill2 (54.8 kgs.) in Figure 10, shows the bulkhead $\lambda_2$ values are 24 mm and 21 □m respectively despite the nearly 40% difference in casting mass. The dominance of the chill over casting mass is further illustrated if we compare the V354-V6 Chill1 to the V354-V6 Chill2, where Chill2 has 50% more contact area which drove a 10 mm drop in $\lambda_2$ values in the bulkhead.

### THERMAL PROCESSING

All the engine blocks investigated in this work either underwent a TSR, quench and then followed by age, or TSR, quench, solution treat (w/o risers), quench then followed by age and is reflected in Figure 11. There is a cost associated with the addition of the solution stage, however in some alloy compositions, not covered in this manuscript, a solution stage may be needed (e.g., 356 and 357 alloys.[1,16,24]). For Cu-bearing alloys work has been done to eliminate the solution treatment but with the aim of achieving the same properties.[11-14] As mentioned, thermal processing is known to have a minimal impact on fatigue performance.[7-9]

The impact of thermal path is being discussed here so that it is not ignored when rendering the best conditions and parameters for a casting that has high fatigue performance as required for automotive applications.

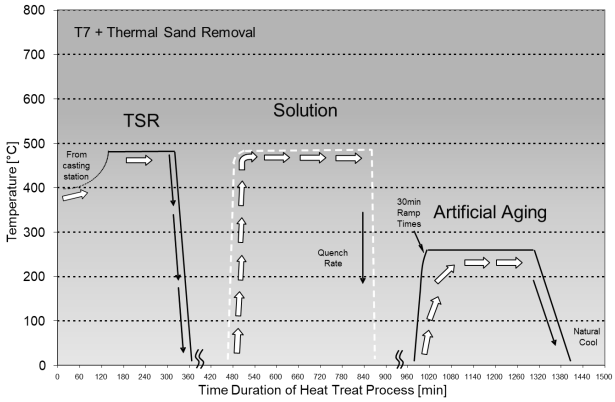


***Figure 11. Thermal path used for the castings outlined in Table 2. Heat treatment parameters specific to each casting are listed in Table 3.***

## DISCUSSION

In short, this manuscript outlines the factors required in process development to achieve high durability bulkhead sections, or any other casting made using the PSCP which uses secondary grade alloys. This becomes increasingly important as lightweighting drives a need for thinner casting sections which can also sustain the high cyclic tensile and compression loads. The key for higher fatigue performance is to have casting sections which have the lowest amount of porosity in terms of maximum pore found and percentage of porosity. The V354-V6-Chill2 + Sr condition, as shown in Figure 7, had the highest fatigue performance due to the fact it has the lowest $\lambda_2$ (Figure 10) which in turn produced the lowest porosity (Figure 9). The target level of Sr at 125 ppm should be used as the higher Sr target used in the V354-I4-Chill2 casting resulted in slightly higher Sr-induced dispersed microshrinkage porosity.

For the U328 alloy, with the shortest freezing range, providing the lowest possible porosity, had not been investigated with a chilled condition and silica sand. Refining the microstructure of the U328 alloy with a chill could also improve the PE values to 1% or higher, permitting roll-forming of bolt holes. In addition, the refined microstructure provided in the chilled bulkhead

allows Fe concentration to be elevated, driving down the raw alloy costs. Sr, as with the V354 alloy conditions with a chill, could be elevated to potentially refine the Si platelet morphology away from the chill, reducing machining costs. The one major drawback for the U328 alloy is that thermomechanical modelling has a larger data-set population for W319 and V354 alloys which provides the necessary resolution in terms of potential failure points (safety factor determination). U328 is not as widely used, and a significant amount of data-set growth would have to be generated to support the thermomechanical modelling of U328 alloy for different casting designs.

Smart chill technology (integrated water cooling) does have the reported ability to reduce porosity further as reported by Farhang Mehr et. al.[26] In this work a cast iron chill in a PSCP (silica sand) investigated water cooling (via integrated channels) of the bulkhead chill before mold filling and at fixed times after mold filling. The alloy used was the V354 alloy. The work identified that a chill preheat was found to have only a small effect on cooling rates between 5 and 50 mm from the chill/casting interface, pour superheat had a moderate effect and staged water cooling had significant effect. This translated into a further drop on porosity which invariably would enhance fatigue performance further. Smart chill technology has not been implemented as there are more complicated designs for the casting station to allow water cooling for the chill.

## CONCLUSIONS

The following conclusions from the current study of casting conditions provide the potential for the highest fatigue performance as demonstrated 8 different precision sand casting iterations.

The key observations are:

- The V354-V6-Chill2+Sr had the lowest $\lambda_2$ and porosity which resulted in the best fatigue performance. The lowest value of $\lambda_2$ was achieved by the mass and contact surface area of the cast iron chill (Chill2) to the bulkhead section of the casting.
- Based on alloy composition, which in turn affects the freezing range which contributes to setting the final porosity, has identified that the U328-V8 has the highest fatigue performance of the non-chilled conditions. This is because the Si and Cu levels of this alloy have the shortest freezing range. It is reasonable to assume that if U328 was used in a chilled condition that further staircase fatigue performance would be realized.
- Additions of Sr can add a significant amount of dispersed microshrinkage which can impair fatigue staircase performance. However, Sr can have a favorable impact on machining characteristics on coarse section of the casting and reduce the severity of gross shrinkage indications in casting sections that cannot be fed or chilled directly. Implementing a chill will drive rapid bulkhead solidification which reduces all the factors that drive pore growth assisted by elevated Sr concentrations.

## REFERENCES

1. Francisco C. Robles-Hernandez, Jose Martin Herrera Ramirez, Robert Mackay, Al-Si Alloys, 1st ed.; Springer: Gewerbestrasse, Switzerland, 2017, pp. 237.
2. J. E. Gruzleski & B. M. Closset, “The Treatment of Liquid Aluminum-Silicon Alloys,” American Foundry Society, Inc., 256pp, 1990.
3. J. Campbell, “An Overview of the Effects of Bifilms on the structure and Properties of Cast Alloys,” *Metallurgical and Materials Transactions B-Physical Metallurgy and Materials Science*, vol. 37B, pp. 857-863, 2006.
4. R. J. M. Kim, H. W. Kwon, & C. R. Loper, “Feeding Behavior of Modified and Unmodified Al-Si Alloys,” *AFS Transactions*, Vol. 98 , pp. 743-749, 1996.
5. K. E. Tynelius, “A Parametric Study of The Evolution of Microporosity in Al-Si Foundry Alloys,” Ph.D. Thesis, *Drexel University*, 1992
6. N. R. Green, J. Campbell, “High Reliability Aluminum Alloy Castings,” *Presented at the 27th ISATA Conference*, Aachen, Germany, (Oct-Nov 1994).
7. J. M. Boileau, J. W. Zindel, & J. E. Allison, “The Effect of Solidification Time on The Mechanical Properties of A356-T6 Aluminum Alloys,” SAE, Paper # 970019, SAE Warrendale, PA, 1997.
8. J. M. Boileau, P. C. Collins, and J. E. Allison, “The Effect of Solidification Time and Heat Treatment on Tensile and Fatigue Testing of a Cast 319 Aluminum Alloy,” SAE, Paper # 980211, SAE Warrendale, PA, 1997.
9. Glenn Byczynski, Robert Mackay, ”The Nemak Cosworth Casting Process Latest Generation,” Shape Casting: *The 10th International Symposium, TMS* (The Minerals, Metals and Materials Society), 2019, (http://doi.org/1007/978-3-030-06034-3_18)
10. R. Mackay & G. Byczynski, “The Use of the Weibull Statistical Method to Assess the Reliability of Cast Aluminum Engine Blocks made from Different Casting Processes,” *Shape Casting: the Fourth International Symposium*, TMS (The Minerals, Metals and Materials Society), 2011, (ISBN: 978-1-11802-937-4).
11. R. Mackay & G. Byczynski, “Methodology to Remove or Scale Back the Solution Treatment in the

Thermal Processing of the 319-Type Alloy Without Changing Material Properties" *International Journal of Metalcasting* (2024). https://doi.org/10.1007/s40962-024-01326-4 (Link last accessed 03-27-25.)

12. G. E. Byczynski & D. A. Cusinato, "The effects of strontium and grain refiner additions on the fatigue and tensile properties of industrial Al-Si-Cu-Mg ally casting produced using the Ford Motor Company – Cosworth precision sand process," *Cast Metals*, 2002, (Vol. 14, pp. 315-324).
13. J. F. Major, "Porosity Control and Fatigue Behaviour in A356-T61 Aluminum Alloy," *AFS Transactions*, Vol. 105, pp. 901-906, 1997.
14. R. Mackay, Elsayed, A. & Byczynski, G. Novel Approach to Thermal Processing Development for Precision Sand Casting Process (PSCP) of Aluminum Engine Blocks, *International Journal of Metalcasting* (2021). https://doi.org/10.1007/s40962-020-00526-y (Link last accessed 03-27-25.)
15. G. Gustafsson, T. Thorvaldsson, & G. L. Dunlop, "The Influence of Fe and Cr on the Microstructure of Cast Al-Si-Mg Alloys", *Metallurgical Transactions A*, Vol. 17A, pp. 45-52, 1986
16. P. N. Crepeau, "Effect of Iron in Al-Si Alloys: A Critical Review", *AFS Transactions*, Vol. 103, pp. 361-366, 1995.
17. F. Paray & J. E. Gruzleski, "Microstructural-Mechanical Property Relationships in a 356 Alloy, Part 1: Microstructure" *Cast Metals*, Vol. 7, Number 3, pp. 29-40, 1994.
18. M. A. Gafur, M. N. Haque and K. N. Prabhu, "Effect of chill thickness and superheat on casting/chill interfacial heat transfer during solidification of commercially pure aluminium," *J. Mater. Process. Technol.*, 2003, 133, (3), 257–265.
19. R. MacKay, M. Djurdjevic and J. H. Sokolowski, "The Effect of Cooling Rate on the Fraction Solid of the Metallurgical Reactions in the 319 Alloy," *AFS Transactions*, Vol. 108, pp. 521-529, 2000.
20. J. P. Anson & J.E. Gruzleski, "A Quantitative Evaluation of the Effect of Hydrogen Content on the Relative Amounts of Shrinkage and Gas Microporosity in a Cast Al-7% Si Foundry Alloy," *AFS Transactions*, Vol. 107, pp.456-467, 1999.
21. J. M. Kim, H. W. Kwon, & C. R. Loper, "Feeding Behavior of Modified and Unmodified Al-Si Alloys," *AFS Transactions*, Vol. 104 , pp. 743-749, 1996.
22. R.I. Mackay & J.H. Sokolowski," Experimental Observations of Dendrite Coarsening & Al-Si Eutectic growth in Progressively Quenched Structures of Al-Si-Cu casting Alloys;" *International Journal of Metalcasting*, Spring 2008, Vol. 2, pp. 57-79.
23. R.I. Mackay, D. Cusinato & J.H. Sokolowski," Chemistry Optimization to Improve Casting Durability of Engine Blocks" *International Journal of Cast Metals Research*, 2010, (Vol. 23, pp. 137-149)
24. J. Gauthier, F. H. Samuel, "Tensile Properties and Fraction Behaviour of Solution Heat Treated 319.2 Al Automotive Alloy," *AFS Transactions*, Vol. 103, pp. 849-855, 1995.
25. Lombardi, A., D'Elia, F., Ravindran, C., MacKay, R., "Replication of Engine Block Cylinder Bridge Microstructure and Mechanical Properties with Lab Scale 319 Al Alloy Billet Castings," *Materials Characterization*, Vol. 87, pp. 125-137 (2014).
26. Farzaneh Farhang Mehr, Steven Cockcroft, Daan Maijer, Robert MacKay, Wade Marquardt, "Assessment of the Impact of Water-Cooled Chill Technology on Microstructure Length-Scales in an A319 Engine Block Casting," COM2017.